Response of a delta-doped charge-coupled device to low energy protons and nitrogen ions

S. T. Lepri
Department of Atmospheric, Oceanic, and Space Sciences, The University of Michigan, Ann Arbor, Michigan 48109

Shouleh Nikzad, T. Jones, and J. Blacksberg
Jet Propulsion Laboratory, California Institute of Technology, Pasadena, California 91109

T. H. Zurbuchen
Department of Atmospheric, Oceanic, and Space Sciences, The University of Michigan, Ann Arbor, Michigan 48109

(Received 30 August 2005; accepted 2 April 2006; published online 19 May 2006)

We present the results of a study of the response of a delta-doped charge-coupled device (CCD) exposed to ions with energies less than 10 keV. The study of ions in the solar wind, the majority having energies in the 1–5 keV range, has proven to be vital in understanding the solar atmosphere and the near Earth space environment. Delta-doped CCD technology has essentially removed the dead layer of the silicon detector. Using the delta-doped detector, we are able to detect H^+ and N^+ ions with energies ranging from 1 to 10 keV in the laboratory. This is a remarkable improvement in the low energy detection threshold over conventional solid-state detectors, such as those used in space sensors, one example being the solar wind ion composition spectrometer (SWICS) on the Advanced Composition Explorer spacecraft, which can only detect ions with energies greater than 30 keV because of the solid-state detector's minimum energy threshold. Because this threshold is much higher than the average energy of the solar wind ions, the SWICS instrument employs a bulky high voltage postacceleration stage that accelerates ions above the 30 keV detection threshold. This stage is massive, exposes the instrument to hazardous high voltages, and is therefore problematic both in terms of price and its impact on spacecraft resources. Adaptation of delta-doping technology in future space missions may be successful in reducing the need for heavy postacceleration stages allowing for miniaturization of space-borne ion detectors. © *2006 American Institute of Physics.*
[DOI: 10.1063/1.2198829]

I. INTRODUCTION

The Sun and the solar wind directly influence the near Earth space environment. Space weather refers to the conditions on the Sun, in the solar wind, and at Earth manifested in the magnetosphere-ionosphere-thermosphere system.[1,2] In order to better understand solar activity and how it affects Earth, we must study a variety of aspects of the Sun and the influence of radiation and the solar wind in the interplanetary medium. The solar wind produces a continuous stream of charged particles that flow away from the Sun in all directions. The solar wind is neither isotropic nor time stationary; occasionally, eruptions on the Sun propagate into the heliosphere via the solar wind. These coronal mass ejections (CMEs) involve the violent ejection of plasma and the frozen-in magnetic field from the Sun into the heliosphere.[3] During the release of a CME, the magnetic field on the Sun abruptly changes its configuration and releases a vast amount of magnetic energy, imparting the energy to the ejected plasma. CMEs have consequences in the near Earth space environment and are often related to enhanced radiation and particle flux and the compression of the magnetosphere.

The identification and study of CMEs have been central to understanding space weather. A host of signatures have been uncovered as identifiers of CMEs in interplanetary space (commonly called interplanetary coronal mass ejections or ICMEs). Some of these signatures include the presence of bidirectional electron (BDE) flows indicating that the observed flow originates on a magnetic loop connected at both ends to the Sun. Additional signatures include velocity and density profiles representative of an expanding feature in the solar wind,[4] certain magnetic field topologies,[5,6] and various ion compositional signatures such as He enhancements and anomalous charge states.[7] Significant variations of the individual ICME identifiers have been observed at 1 astronomical unit (AU). Unlike most other signatures, ion compositional signatures are independent of radial distance from the Sun as well as plasma interactions. Beyond three to four solar radii, the solar wind density is too low for ionization and recombination to occur. These characteristics make ion compositional signatures ideally suited for the identification of ICMEs over a large range of heliospheric distances.

Recently, it was shown that elevated Fe charge states are an excellent tracer of ICME material in the solar wind.[8,9] Figure 1 shows an example where the observed average charge state of Fe approaches 16+ and above during an ICME in September of 1998. Since the typical charge state of Fe in the solar wind is ~9–10+, this elevated charge state

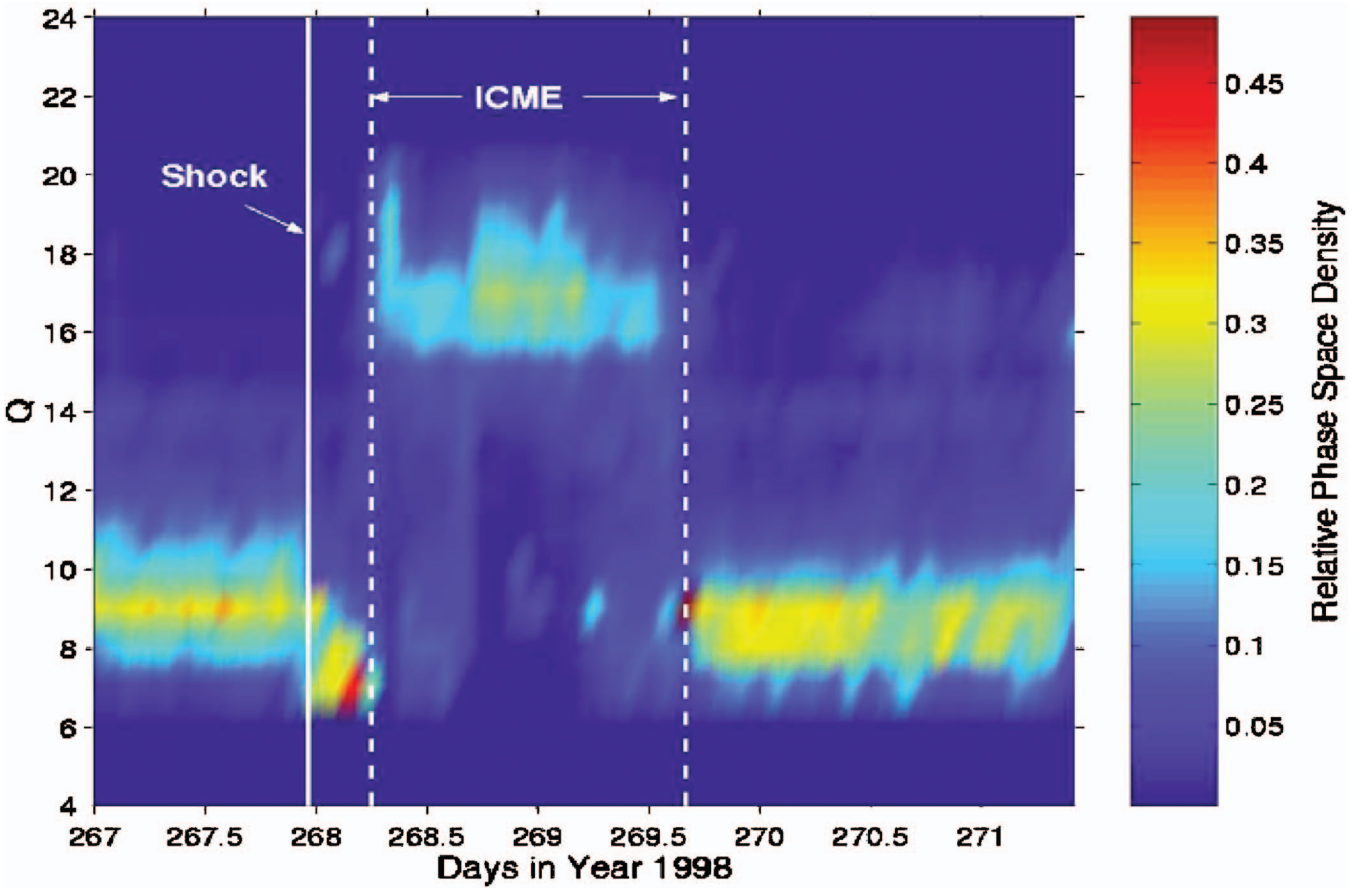

FIG. 1. (Color) This panel shows solar wind charge states of Fe as a function of day of year (DOY) observed in 1998 using the ACE SWICS instrument. The shading represents the relative abundance of the charge states (summing to one for each time step). Fe charge states approximately nine to ten are expected in quiet solar wind. Charge states >12.0, especially those ~ 16.0, are indicative of hot material associated with ICMEs. The period above marked by the dashed lines marks the observation of high charge states of Fe ($Q_{\mathrm{Fe}} > 16$) during an ICME passage at the ACE spacecraft at L1. The ability to resolve charge and mass of ions in the solar wind allows us to learn about the conditions close to the Sun during a CME eruption.

indicates an unusually hot source. Knowledge of the charge states in the solar wind cannot only help us identify ICME material but can also give us vital insight into the processes and conditions close to the Sun, where the ICME originated. Measurements such as those highlighted in Fig. 1 show the need for detectors that can identify ions in the solar wind.

The solar wind ionic composition spectrometer (SWICS) on the Advanced Composition Explorer (ACE) was used to obtain the above data and represents the most comprehensive measurements of the solar wind composition to date.[10] As hinted to above, the ion composition of the solar wind varies according to the nature of its source on the Sun and processes that take place on and near the Sun. The many ions in the solar wind are characterized by varying mass, charge, and energy. SWICS is able to determine these quantities using a combination of energy per charge (E/Q) analysis, velocity (v) measurement in a time-of-flight (TOF) region, and total energy (E) measurement in a solid-state detector (SSD). The total energy measurement is the most difficult due to the energy threshold necessary for accurate measurements of E.

This article discusses the proof of concept application and analysis of a solid-state particle detector technology to overcome these problems. This detector was developed by Nikzad *et al.*,[11] and is sensitive at much lower energies than traditional solid-state detectors. These detectors were initially developed by Hoenk *et al.*[12] for applications in ultraviolet (UV) detection. Nikzad *et al.*[13] presented single-event detection of protons with a delta-doped charge-coupled device (CCD) and later, Jewell *et al.*[14] demonstrated molecular and atomic ion detection qualitatively. Here, we present the first quantitative observations with this detector, of ions heavier than protons. We have launched a quantitative and analytical study of the response of a delta-doped CCD as a particle detector at energies down to 1 keV. We begin by discussing technology currently operating in space and its limitations. We then describe the delta-doping process and its implications for extending the detection limit. Subsequently we discuss the laboratory testing and finally discuss the results and the possible application of this technology to spaceborne detectors.

II. CURRENT SPACE-BASED PARTICLE DETECTION

Solid-state detectors have many desirable features; they are compact, robust, and relatively inexpensive, with high resolution and low power consumption.[15] They are unique in that they produce a signal proportional to the incident particle energy. Therefore, one can determine the energy, incidence rate, and positional information of each incident particle individually. Implementation of early SSDs in space

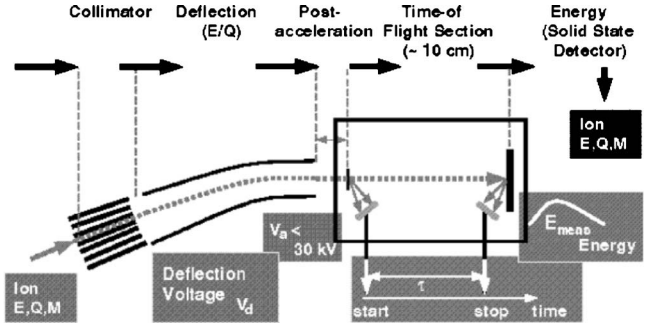

FIG. 2. Schematic of measurement technique used in the SWICS instrument on ACE. Adapted from Gloeckler *et al.* (Ref. 10). The quantity V_d, the deflection voltage, is set to select ions with certain energy per charge, E/Q. Instruments such as this are key to solar wind observations but are currently inhibited by SSDs with low energy thresholds ~30 keV.

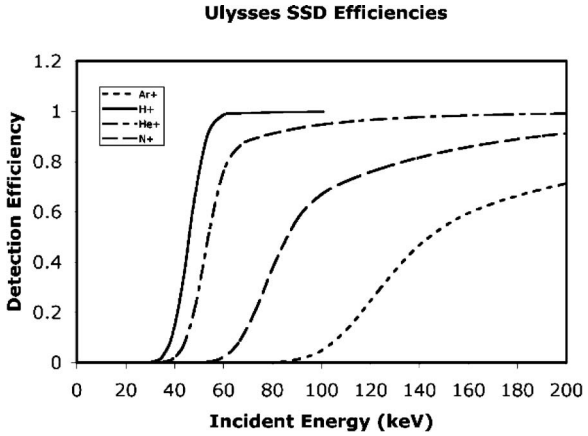

FIG. 3. Solid-state detector efficiency curves for SWICS on the Ulysses spacecraft. The curves were fitted to laboratory calibration data. The efficiency depends strongly on mass (Ref. 19).

applications in the early 1960s enabled the measurement of high energy ions in the heliosphere. By pairing a SSD with another type of sensor, for example, an electrostatic analyzer, the resulting instrument was able to cover a broader energy range and particle identification became possible (Ref. 16 and references therein).

SWICSs on Ulysses and ACE are the first sensors of their type that can unambiguously identify almost 40 heavy ions and obtain charge state distributions and abundances for ten elements.[10,16] SWICS measures the elemental and isotopic compositions of the solar wind in unprecedented detail.[10] SWICS resolves the threshold limitations by using a postacceleration voltage. The operation of this instrument will now be described in detail.

The SWICS sensor identifies ions by measuring a combination of three quantities: E/Q in the electrostatic deflection region, v in the TOF region, and E in the SSD (Ref. 10 and references therein). Figure 2 shows a schematic of the operation principle for the SWICS instrument. Solar wind ions of kinetic energy E (usually several keV), charge Q, and mass M, with the proper entrance trajectories, enter the sensor through the large-area multislit collimator. They then enter the curved deflection analyzer that serves as an energy per charge (E/Q) filter by stepping through a range of deflection voltages (V_d), and also as an UV trap for background photon rejection. The E/Q filter is stepped through voltages, allowing only ions with the appropriate energy per charge to pass into the TOF energy system. Before entering the TOF system, the ions are postaccelerated by a ~25 kV potential. The ions then encounter a carbon foil after postacceleration and before entering the TOF system. As the ion passes through the carbon foil, secondary electrons are emitted. The ions need a minimum initial energy between 5 and 10 keV to pass through the carbon foil. The secondary electrons experience the weak electric potential (~1 kV) in the TOF region that steers them to a microchannel plate (MCP) detector, where they are detected and generate a start signal.[17] The postacceleration gives the ions enough energy to pass through the carbon foil and to trigger the solid-state detector. At the other end of the TOF system (~10 cm in length), the particle impacts the gold front surface of the ion implanted solid-state detector, emitting more secondary electrons that are accelerated and detected by a second MCP where they generate a stop signal. The time delay between the start signal and the stop signal is measured and constitutes the time of flight, τ. The residual energy, E_{meas}, of the particle is measured in the solid-state detector, allowing the particle to be identified. The measurements of E_{meas}, τ, and E/Q (determined by the voltage step setting on the electrostatic analyzer), in addition to knowledge of the postacceleration voltage U_a, enable the determination of mass M, charge state Q, and incident energy E (equivalently incident speed, V_{ion}). The equations used to determine these values are

$$M = 2\left(\frac{\tau}{d}\right)^2\left(\frac{E_{\mathrm{meas}}}{\alpha}\right),$$

$$Q = \frac{E_{\mathrm{meas}}/\alpha}{(U_a + E/Q)\beta} \approx \frac{E_{\mathrm{meas}}/\alpha}{U_a},$$

$$M/Q = 2\left(\frac{\tau}{d}\right)^2 (U_a + E/Q)\beta \approx 2\left(\frac{\tau}{d}\right)^2 U_a,$$

$$E_{\mathrm{ion}} = Q(E/Q),$$

$$V_{\mathrm{ion}} = 438[(E/Q)/(M/Q)]^{1/2},$$

where d is the distance the ions travel through the TOF region, β takes into account the small energy loss of the ions as they pass through the carbon foil, and α is the nuclear defect which is related to the ratio of measured energy in the SSD to the kinetic energy incident at the detector in the solid-state detector.[18] The units for V_{ion} are in km/s, E/Q in keV/e, and M/Q in amu/e.

Ulysses SWICS was launched in 1990 and is currently in a highly inclined elliptical orbit about the Sun. ACE SWICS was launched in 1997 and orbits the Sun at the first Lagrangian point, which is the gravitational saddle point along the Earth-Sun line. The Ulysses SWICS solid-state detector detection efficiencies are modeled from calibration data[19] and are plotted in Fig. 3. The lower detection efficiencies for heavier ions are likely due to the pulse-height defect (see Ref. 15 for definition), including dead layer losses, losses to nuclear collisions, and recombination within the device at

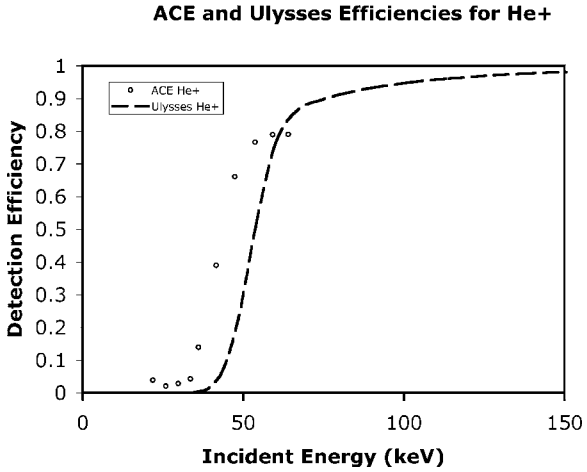

FIG. 4. Solid-state detector efficiencies for He^+ for the ACE and Ulysses spacecraft. Improved technology for the ACE mission allows He^+ to be detected at lower energies compared to the Ulysses SSD. However, ions below 25 keV still elude detection.

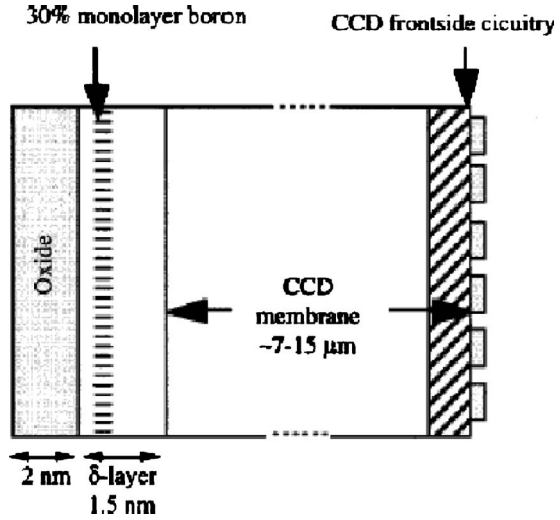

FIG. 5. Schematic of delta-doped CCD structure (not to scale) showing boron atoms 0.5 nm below the silicon epilayer surface and protected by an oxide overlayer. Delta-doped CCDs are back-illuminated devices, meaning that particles are incident on the back surface. [Adapted from Nikzad *et al.* (Ref. 13).]

interfaces or intrinsic defects. At higher energies, recombination can also occur along the dense plasma track created by a heavy ion.

A thin-window ion implanted silicon SSD, with a nominal window thickness of 200 Å,[20] was used in instruments for the ACE spacecraft. The thin-window nature of the ACE SSD reduces the dead layer from the previously implemented detector used on Ulysses. Ion implanted detectors have a crystal structure that is less disturbed, more stable, and less affected by ambient conditions than surface barrier detectors.[15] Figure 4 shows the experimental helium efficiencies from ACE (circles) and the modeled efficiencies from Ulysses (dashed). The ACE curve shows improved detection efficiency at lower energies, as should be expected for the thin-window SSD; however, helium ions with less than 30 keV are still not detectable. The ACE curve also stops around 60 keV where measurements were no longer obtained.

III. DELTA-DOPED DETECTOR TECHNOLOGY

The Jet Propulsion Laboratory (JPL) has performed extensive research with the intent to decrease the low energy particle detection threshold of silicon detectors. This breakthrough technology is the development of a process that is applied to fully processed silicon detectors such as CCDs to enable detection and imaging of both low energy electrons and molecular ions with energies down to 1–2 keV.[12,14,21] CCDs are two-dimensional arrays as large as 16 megapixels and have many advantages over conventional SSDs, phosphors, or position sensitive photon detectors.[21]

CCDs are typically used for detection and imaging of photons and are usually operated by exposing the front side [very large scale integrated (VLSI)-fabricated side] of the detector to either electromagnetic radiation or particles for a certain length of time, i.e., exposure time. During this time period, charge is created and is stored in the corresponding pixel. When the exposure is completed, parallel clocks vary voltages in a controlled manner moving the charge packets stored in each pixel along the parallel register toward the serial register. Once the signal is in the serial register, the serial clocks vary the voltages along the serial register and the charge packet moves toward the readout electronics.

Front side illumination of these CCDs limits low penetrating ionizing radiation detection due to absorption in the polycrystalline Si gates (~5000 Å—see Fig. 5 for an illustration). To remedy this insensitivity, backside illumination can be employed. Typically, backside illumination requires thinning of the device in order to bring the backside of the surface closer to the front side collection well. However, without any further processing, carriers generated in the back illumination are trapped near the back surface due to unfavorable band bending at the surface. Therefore, such a thinned CCD is still insensitive to ionizing radiation that generates electron-hole pairs at or near the back surface.[21] Hoenk *et al.*[12] developed the delta-doping technology that eliminated these losses for UV detection and Nikzad *et al.*[21,22] applied this technology for particle detection. Using the delta-doped CCDs, UV photons have been imaged with 100% internal quantum efficiency (QE).[11,12] Delta doping has resulted in 100% internal QE in thinned back-illuminated *n*-channel (*p*-type) CCDs over the entire spectral range from soft x rays through extreme ultraviolet (EUV), UV, and visible wavelengths (Ref. 23 and references therein). While the delta-doping technique was developed at JPL to modify the band structure of thinned back-illuminated *n*-channel silicon CCDs initially for enhancement of response in the ultraviolet, similar processes are at various stages of development for p-i-n diode arrays,[24] complementary metal-oxide semiconductor (CMOS) arrays,[25] and *p*-channel CCDs.[26(a),26(b)] In addition, delta-doped CCDs have been able to detect electrons with energies as low as 50 eV,[22] and protons with energies ranging from 1.2 to 12 keV,[13] and more recently other atomic and molecular ions with ~700 eV energy.[14]

Achieving the maximum possible QE in silicon detector arrays requires back illumination and a suitable back surface treatment. The ideal back surface treatment must passivate

the silicon surface in order to eliminate excess surface-generated dark current and create a near-surface electric field that prevents surface recombination and drives photogenerated carriers toward the front-surface collection well. Using molecular beam epitaxy (MBE) to grow an ultrathin layer of highly doped silicon achieves these essential objectives by creating a "sheet" of charge just a few atomic layers beneath the silicon surface. This layer produces a fixed potential in the crystal that effectively "pins" the surface band structure and stabilizes the CCD against potential sources of hysteresis and instability (such as, for example, hysteretic population of surface states caused by environmental contamination, radiation damage, and prior illumination). Named "delta doping," after the mathematical delta function and the doping profile of a single, ultrahigh doping density layer immediately below the surface, this process modifies silicon arrays to achieve optimal QE and dark current. The characterization of delta-doped CCDs shows that the measured QE is exactly what expected if the only loss is due to reflection of photons from the surface. This optimal, reflection-limited response is referred to as 100% internal QE because all photons that are absorbed into silicon and generate carriers are detected.

Because for the entire UV spectrum (from 100 to 380 nm), the absorption length of photons in silicon is ~40–100 Å, the 100% internal QE indicates detection of carriers generated within this range and thereby suggests very little or no dead layer (dead layer less than 40 Å). A dead layer less than 40 Å is suggested by the 100% internal QE for UV photons whose absorption length in silicon is 40–100 Å. In conventional CCDs, a backside potential well is created when positive charge becomes trapped at the Si/SiO_2 interface of a bare silicon surface; this region will trap electrons generated near the surface. The reduction of this backside potential well will eliminate the electron trapping at the back surface and will result in the ability to detect particles with ranges greater than 0.5 nm in silicon, thus enabling the detection of low energy particles. The stability of delta-doped detectors' response has been measured by various groups as a function of time,[27] temperature, UV illumination history, and ambient gases[23] with no observed change in the UV quantum efficiency. Testing the quantum efficiency in the UV has been shown to be a good measure of the stability of the delta-doping process.

For the measurements described in this article, 1024×1024 pixel CCDs were thinned to a 12 μm thickness at JPL using chemical processes by successive etching using KOH and a mixture of hydroflouric/nitric/acetic acids[28] and delta doped by using processes described in Ref. 12. Briefly, in the delta-doping process, MBE is used to grow 1.5 nm of single-crystal silicon on the backside of the CCD, while incorporating a sheet of 2×10^{14} boron atoms/cm^2 (nominally a single monolayer of the crystal) at a precise location of 0.5 nm from the backside surface.[12]

The exact value of the energy threshold of a solid-state detector is largely determined by four factors: (1) energy loss of particles in the dead layers of the silicon detector, (2) recombination of electron-hole pairs at the dead layer interface, (3) capacitance of the detector, and (4) rms noise of the electronics design. The delta-doping technology remedies factors (1) and (2). The application of this technology to a pixilated solid-state detector, such as a CCD, would reduce the capacitance and noise in the system remedying factors (3) and (4). The rest of this article will focus on the proof of concept of delta-doped detectors as particle detectors for heavy ions. We will conclude by discussing future steps that need to be taken in order to adapt this technology to a detector that could be utilized in a possible flight instrument for solar wind composition analysis or other lower energy ion analysis.

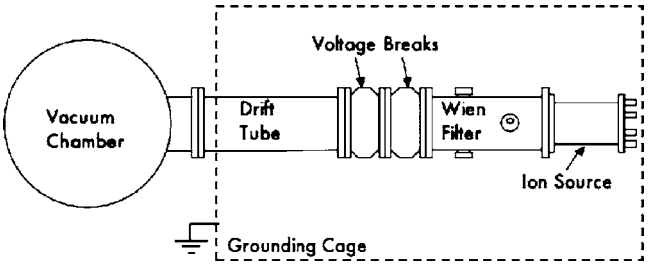

FIG. 6. Experimental setup (not to scale).

IV. LABORATORY CHARACTERIZATION OF THE CCD

In order to calibrate and test the thinned, backside illuminated, delta-doped CCD's response to ions with energies less than 20 keV, experiments were performed by exposing it to a mass selected ion beam at the calibration facility at the University of Michigan (UM) Department of Atmospheric, Oceanic and Space Sciences. The experimental setup consisted of a large cylindrical vacuum chamber attached by a drift tube to an ion source and Wien filter. Two voltage breaks were located between the Wien filter and the drift tube. Figure 6 shows a schematic of the experimental setup.

The ion beam was produced by an electron-impact ion source that was custom built at the University of Maryland; mass selection of the beam was done using a Wien filter purchased from the Colutron Research Corporation. In general, we set the extraction voltage from the ion source at 1 keV. At this energy, the Wien filter can efficiently disperse the separate masses ($M/\Delta M = 400$ according to the manufacturer). The ion beam is accelerated to its final energy after the Wien filter; the beam can be tuned from 1 to 20 keV.

The detector used in our experiments was the delta-doped 1024×1024 12 μm pixel originally fabricated at Loral-Fairchild for NASA's Cassini mission. A Faraday cup, whose efficiency is assumed to be unity, was used to measure the beam current. The aperture of the Faraday cup was circular with an area equal to 0.254 cm^2. The CCD had a detecting surface that is 1 cm^2. The CCD was masked with an aluminum plate with an aperture identical to the aperture of the Faraday cup, eliminating uncertainties that arise from structure in the beam. The Faraday cup was upstream from the CCD and the flux falloff due to the ~6° angular dispersion of the beam was taken into account during the calibration. The beam current was stable within 1% during the CCD measurements. The mode of operation and the characteristics of the CCD allowed particle detection well below the saturation level, or full well capacity, for this CCD.[15]

The experiment was conducted under high vacuum with pressures around 5×10^{-7} Torr. The Faraday cup was situated 170 cm downstream from the ion source. The CCD was mounted 184 cm downstream from the ion source on a stationary copper rod and was operated at room temperature.

No bias was applied to the CCD; only the internal electric field due to charge separation was used to move charges into the front side collection well. In this mode, the detector exhibits poor frequency response due to the larger capacitance and the low electric field. One could apply a reverse bias to the CCD that would increase the depletion region, or active area of the detector.[29]

In current-mode detection, the CCD can be operated such that the entire signal collected over the surface of the exposed portion of the detector is integrated and read out through only the two output amplifier pins into an electrometer. By integrating over all the exposed pixels in the CCD, the pixel-to-pixel variations are averaged out. Comparing the incident current (I_{inc}) to the detected current (I_{meas}), one can obtain a measure of the QE,[22] analogous to the photon quantum efficiency,

$$\frac{I_{\text{meas}}}{I_{\text{inc}}} = QE = T^{*}QE_{\text{int}}{}^{*}QY,$$

where T, which is a function of incident ion energy, is the transmittance of ions into the silicon, and accounts for the surface scattering and absorption in surface oxides or other applied coatings. For heavier ions and ion beams that are incident normal to the detector surface, the effects of surface scattering will be negligible. Quantum yield is defined for an ideal interaction as $QY=E_0/E_{\text{eh}}$, where E_0 is the incident energy and E_{eh} is the electron-hole pair formation energy, $E_{\text{eh}}=3.62$ eV per electron-hole pair (at 300 K) for higher energy particles and x rays (Ref. 13 and references therein). Thus, it is the conversion efficiency of ion energy deposition into electron-hole pair creation. The internal quantum efficiency, QE_{int}, is defined as the number of electron-hole pairs collected versus the number produced.

The QE measurements of the CCD were made by measuring the current produced in the CCD by the incident ions and comparing it with the incident ion flux measured by the Faraday cup. Flux measurements using the Faraday cup were performed before and after each CCD measurement to account for any instability or drift in the incident ion flux. The Faraday cup currents were read out by a Keithley 486 picoammeter. The background current at the Faraday cup exhibited periodic fluctuations $\sim$0.05 pA.

For each measurement, the Faraday cup was moved into the beam using the *X-Y* stage and multiple readings were recorded. The picoammeter averaged the data using a repeating average to achieve a good signal to noise ratio. Next, the Faraday cup was moved out of the beam path, exposing the CCD. The CCD current was measured by the Keithley 6514 electrometer and multiple readings were recorded. After turning the beam off, by setting the extraction voltage on the ion source to zero, multiple measurements of the background were recorded. Since the CCD is sensitive to light, the light from the ion source filament, ion gauge filament, and ambient room light that leaked into the system through the nonopaque ceramic voltage breaks all contributed to the background level measured by the CCD. The beam was restored and multiple measurements were recorded from the CCD again. The Faraday cup was then moved back into the beam and multiple readings were again recorded. By taking beam calibration measurements before and after the CCD measurements, we can account for any drift in the beam current over time.

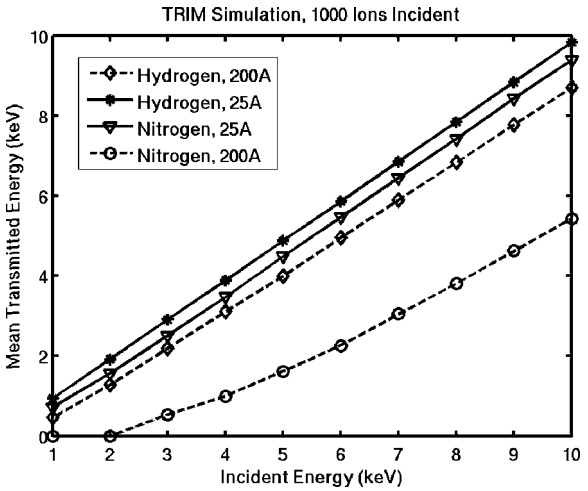

FIG. 7. Mean transmitted energy as a function of incident energy of 1000 ions incident on a hypothetical dead layer. The solid lines represent the results from the thin, 25 Å dead layer, while the dashed lines represent the results from the thicker, 200 Å dead layer. Both H^+ and N^+ lose more energy in the thicker dead layer; however, N^+ loses much more in the thicker layer and is no longer detectable at or below 2 keV. In the thicker dead layer, N^+ loses half of its incident energy.

Before we present the results from our experiments, let us consider the following simulation. In order to illustrate the improved detection capabilities of the delta-doped detector, we examined several stopping and range of ions in matter (SRIM) simulations that calculated the energy lost by 1000 ions as they traveled through a hypothetical dead layer.[30] Delta-doped detectors have $\sim$20 Å of oxide on the lattice-registered delta-doped detector; we simulated a delta-doped detector with a 25 Å oxide (a conservative number) on a silicon target. For comparison, we simulated the dead layer of the commercial SSD used in ACE SWICS with a reported 200 Å oxide layer on silicon.[20] We plot the transmitted energy as a function of incident energy for both hydrogen and nitrogen in Fig. 7. The solid lines represent the results for the thinner layer (25 Å for the delta-doped CCD) and the dashed lines represent the results for the thicker layer (200 Å for the SWICS-type SSD). Hydrogen into 200 Å is plotted as diamonds on the dashed curve, while hydrogen into 25 Å is plotted as stars on a solid curve. Nitrogen into 200 Å is plotted as open circles on a dashed curve and nitrogen into 25 Å is plotted as upside-down triangles on a solid curve. The mean transmitted energy was calculated from the distribution of ions that were transmitted through the simulated dead layer. It is evident that the ions lost more energy in the thicker dead layer, with the results for nitrogen being the most pronounced. Nitrogen at or below 2 keV was not detected in the 200 Å layer. In the 25 Å layer, nitrogen passes

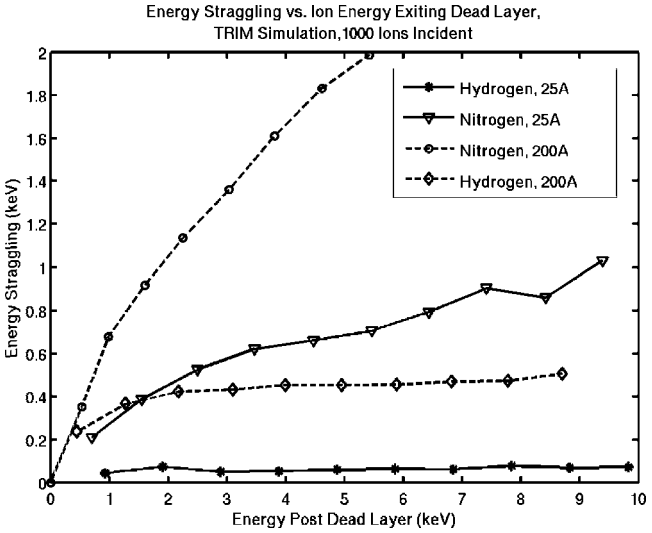

FIG. 8. Energy straggling as a function of transmitted energy. The solid lines represent the thinner dead layer, while the dashed lines represent the results for the thicker dead layer. Both the H^+ and N^+ exhibit much larger energy straggling in the thicker dead layer. The energy straggling for H^+ in the thin dead layer is nearly negligible.

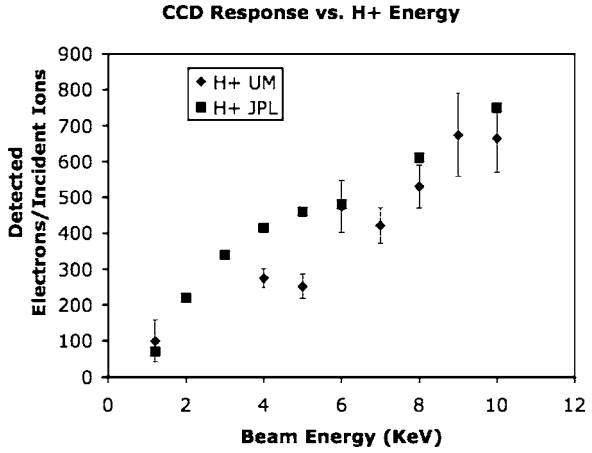

FIG. 9. The response of the delta-doped CCD to H^+ beam. The squares represent the data obtained by JPL in 1999 using the CCD in imaging mode to detect individual protons (Ref. 13). The diamonds represent our data obtained in this study using the CCD in current mode.

with most of its incident energy still in tact, comparable to that from hydrogen.

Figure 8 shows the mean energy straggling in the dead layer versus the mean transmitted energy the particles retain when they exit the dead layer. The dashed lines once again represent the thicker dead layer results, while the solid lines represent the thinner dead layer results. Both the hydrogen and the nitrogen ions exhibit enhanced energy straggling in the 200 Å layer, while the straggling is greatly reduced in the 25 Å layer.

These simulations illustrate that the thinner dead layer allows particles to pass through retaining much of their incident energy, which can then be deposited and measured in the active area of the detector. Delta-doping technology is able to increase the sensitivity of silicon detectors at much lower energies, by reducing the dead layer and the losses in the dead layer. Particles that enter a delta-doped detector retain most of their original energy. Lower energy particles will produce a more measurable response in the delta-doped detector as opposed to the conventional SSD, which exhibits insurmountable difficulty in detecting low energy heavy ions.

The first set of detection measurements we present is for H^+. In order to ensure the validity of our measurements, we reproduced the published measurements from Nikzad *et al.*[13] In the 1999 measurements of H^+, the delta-doped CCD was operated in imaging mode and exposed to an extremely low flux of protons. The low flux enables the observation of individual particles. While operated in imaging mode, the detector had an applied reverse bias across the depletion region, hence increasing the width of the active area; this decreases the capacitance of the detector and the noise levels. Since the measurements presented here were executed without an external bias, the active region was more limited, which may cause our results to differ slightly from the 1999 JPL measurements.

The H^+ data are shown in Fig. 9. The QE of the CCD is plotted against the incident beam energy. Our data (diamonds) are plotted along with those from the results (squares) of Nikzad *et al.*[13] This figure shows general consistency between the two sets of measurements. The two data sets show similar trends and highlight the ability to detect low energy hydrogen with this detector. The response is calculated by first subtracting the background signal on the CCD due to ambient light from the signal during ion illumination. This gives us the current signal due to the ions integrated over the surface of the CCD. Then, the current can easily be reduced into the output current due to electron-hole pair formation by the incident ions. In order to determine the incident flux at the CCD, the flux at the Faraday cup is measured and propagated to the CCD by integrating the beam profile at both the Faraday cup and the CCD and accounting for the difference due to the spreading of the beam away from the source. This translated into the CCD receiving 94% of the flux observed at the Faraday cup. The CCD current divided by the corrected incident ion flux or current (since their apertures are the same area) is the detected number of electron-hole pairs produced per incident ion. In the absence of surface losses, backscattering, or detector inefficiencies, this number should approach the statistical average that has been measured for higher energy photons and particles, i.e., one electron-hole pair per every 3.62 eV of incident ion energy.

For a 1 keV proton, the statistical average number of electron-hole pairs predicted by the linear relationship (validated previously at higher energies) is 278. It can be seen from Fig. 9 that ~100 rather than 278 electrons have been created in the delta-doped CCD. However, delta-doped CCDs in general[11] and the CCD used in this article have exhibited 100% internal quantum efficiency in the UV, suggesting 100% collection efficiency. Although the detector is not reverse biased, delta doping creates a small built-in field at the detector surface.[22] However, this built-in field does not extend throughout the entire epilayer and therefore the majority of this region is field-free. At low energies, most particle interactions occur near the surface of the detector. Lateral diffusion by generated electrons in this region may result

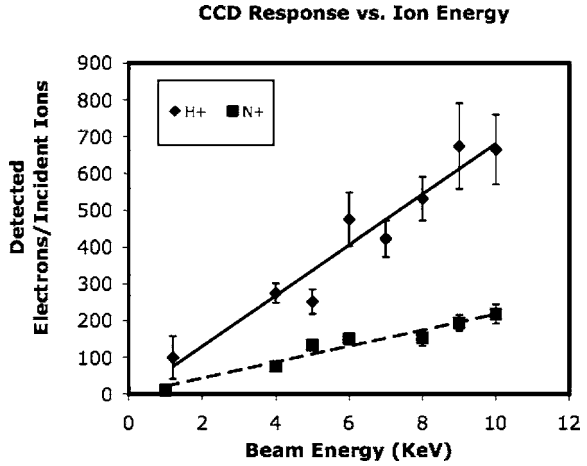

FIG. 10. The response of the CCD to H^+ and N^+ beams. The H^+ results from Fig. 9 are plotted on this figure as diamonds. Our N^+ results are plotted as squares. The response to the N^+ beam is lower than for the H^+ beam, as expected from the simulations.

in recombination of the electron-hole pairs before they are detected.[13] Additionally, the particles used in this study created electron-hole pairs that should experience the same built-in fields as those created by UV photons. However, the distinction between the two cases is that a much higher concentration of electron-hole pairs is created by the charged particle. The recombination process is proportional to the concentration of both electrons and holes. We conjecture that for each incident ion, the 278 pairs of holes and electrons are reduced to around 100 by rapid recombination that takes place before they can be separated by the built-in field.[13] The effect of the field-free region on the device response to particles will be investigated by conducting similar experiments using recently developed fully depleted delta-doped arrays.[25]

Measurements were also obtained for N^+ using the same methods discussed above for H^+. Figure 10 shows the results of these measurements by plotting the QE against the incident N^+ (squares) beam energy, along with the previous results for H^+ (diamonds). The N^+ signal obtained by the CCD due to the impact of N^+ ions is lower than that for H^+. A similar relationship is observed above in the efficiencies of the SWICS solid-state detector on Ulysses (see Fig. 3). It has also been observed at these energies that higher mass particles have larger nuclear defects.[31] Another factor contributing to the observed difference may be lateral diffusion of electrons in the field-free region that recombine before being detected.[13]

V. DISCUSSION

These results indicate a drastic improvement in the ability to detect low energy ions. This is especially important for instruments used in space science. As shown in Fig. 3, the solid-state detectors used in the SWICS instruments on ACE and Ulysses have detection thresholds near 30 keV for protons. Here, we have demonstrated the ability to detect H^+ and N^+ ions with energies between 1 and 10 keV.

Our SRIM simulations illustrate the contrasting penetration limits of the particles in the delta-doped CCD and the SSDs currently utilized in composition detectors in space. The thickness of the detector's dead layer determines whether a particle may be sensed.

It is worthwhile to compare these results to recent work by Funsten *et al.*[31] in which they measure the nuclear defect in 100% quantum collection efficiency silicon photodiodes with very thin windows (40–60 Å). Using current mode detection, they examined the response of the SSD to a wide range of ions from H^+ to Ar^+. Similar to the results obtained by Funsten *et al.*, we demonstrate detection of low energy ions down to 1 keV. The difference in absolute signal obtained from these two approaches is under further investigation. The ability to directly detect low energy particles with solid-state detectors marks a significant step in improving space plasma instruments.

We have quantitatively measured the QE and discussed the applicability of the delta-doped CCD as a heavy ion detector. We reproduced the QE of the CCD in current mode to H^+ ions with energies between 1 and 10 keV, previously measured by the Nikzad *et al.* in imaging mode.[13] In addition, we have extended the study to include new measurements of N^+ ions in the same energy range. We have compared the energy transmission of 1 keV particles in the delta-doped CCD and the conventional SSD through the use of SRIM simulations. These simulations highlight the dramatically enhanced transmission that is possible with delta-doped silicon detectors. The thin dead layers preserve the majority of particles' incident energy and reduce the energy straggling of particles as they pass through the layer. Particles that were undetectable in the conventional SSDs' dead layer are detected with the delta-doped detector and retain much of their incident energy.

Detectors used in solar wind composition instruments should fulfill a certain set of requirements. Detectors used in space applications should have the ability to resolve nanosecond pulses. Standard CCDs with multimegapixel formats are normally read out in milliseconds, indicating that using a standard CCD would not be ideal for ion detection in the solar wind. Because of this timing requirement, a pixilated delta-doped SSD, with between four to six pixels and a readout in nanoseconds, needs to be developed.

Successful detection of H^+ and N^+ ions below 10 keV will have tremendous implications for space science and future solar wind measurements. Satellites such as ACE and Ulysses and their ion-composition spectrometers are currently returning the most detailed data on solar wind composition ever observed. However, their science return is still limited by their particle detectors—especially for low energy ions. The delta-doped detector's increased detection range and sensitivity, along with low-noise electronics and reduced capacitance, will be far more effective than the current detectors flown in space. The delta-doping technology remedies two of the four factors that largely determine the energy threshold of a SSD by effectively eliminating the dead layer. By applying delta-doped technology to a fast readout pixilated solid-state detector with reduced capacitance and noise remedying the remaining limitation of solid-state detectors, i.e., large capacitance of the detector, and rms noise of the electronics design. The resulting detector would allow for quality measurements with reduced mass, power require-

ments, and cost for the instrument payload. In the future, tests of this delta-doped technology in a CCD or other detector structures, especially fully depleted delta-doped arrays, should be performed in pulse height mode to further examine its ability to detect individual low energy ions[13] with high resolution of ion energy. Implementation of a solid-state detector with delta-doped technology would minimize the voltage needed to accelerate particles above the low energy threshold and the associated high voltage shielding. By taking advantage of these advancements in solid-state low-energy particle detectors, compact space plasma instruments with improved capabilities can be realized.

ACKNOWLEDGMENTS

The authors would like to thank A. Jewell for her assistance and M.E. Hoenk and T. Elliot for many helpful discussions. In addition, the authors would like to thank P. Koehn for laboratory support, J. Raines for providing the ACE efficiencies, and R. Lundgren for useful discussions regarding current space detector technologies. This work was funded in part by the NASA Graduate Student Researchers Program and the JPL Director's Research and Development Fund.

[1] D. N. Baker, Adv. Space Res. **22**, 7 (1998).
[2] D. G. Cole, Space Sci. Rev. **107**, 295 (2003).
[3] E. R. Priest, Astrophys. J. **328**, 848 (1988).
[4] J. T. Gosling and P. Riley, Geophys. Res. Lett. **23**, 2867 (1996).
[5] L. F. Burlaga, *Physics of the Inner Heliosphere* (Springer-Verlag, New York, 1991), Vol. 2, pp. 1–22.
[6] J. T. Gosling, in *Physics of Magnetic Flux Ropes*, *Geophysical Monograph Series*, edited by C. T. Russell, E. R. Priest, and L. C. Lee, Vol. 58 (American Geophysical Union, Washington, D.C., 1990), p. 343.
[7] G. Borrini, J. T. Gosling, S. J. Bame, and W. C. Feldman, J. Geophys. Res. **87**, 7370 (1982).
[8] S. T. Lepri, T. H. Zurbuchen, L. A. Fisk, I. G. Richardson, H. V. Cane, and G. Gloeckler, J. Geophys. Res. **106**, 29 (2001).
[9] S. T. Lepri and T. H. Zurbuchen, J. Geophys. Res. **109**, 112 (2004).
[10] G. Gloeckler *et al.*, Space Sci. Rev. **86**, 495 (1998).
[11] S. Nikzad, M. E. Hoenk, P. J. Grunthaner, R. W. Terhune, and F. J. Grunthaner, Proc. SPIE **2198**, 907 (1994).
[12] M. E. Hoenk, P. J. Grunthaner, F. J. Grunthaner, R. W. Terhune, M. Fattahi, and H. Tseng, Appl. Phys. Lett. **61**, 1084 (1992).
[13] S. Nikzad, D. Croley, S. T. Elliot, T. J. Cunningham, W. K. Proniewicz, G. B. Murphy, and T. J. Jones, Appl. Phys. Lett. **75**, 2686 (1999).
[14] A. D. Jewell, T. J. Jones, M. P. Sinha, and S. Nikzad, Appl. Phys. Lett. **88**, 043501 (2006).
[15] G. F. Knoll, *Radiation Detection and Measurement* (Wiley, New York, 2000).
[16] G. Gloeckler *et al.*, Astron. Astrophys., Suppl. Ser. **92**, 267 (1992).
[17] G. Gloeckler and K. C. Hsieh, Nucl. Instrum. Methods **165**, 537 (1979).
[18] F. M. Ipavich, R. A. Lundgren, B. A. Lambird, and G. Gloeckler, Nucl. Instrum. Methods **154**, 291 (1978).
[19] R. Von Steiger *et al.*, J. Geophys. Res. **105**, 27 (2000).
[20] G. Ho, University of Maryland Technical Report No. TR 1994-9-7, 1994.
[21] S. Nikzad, A. L. Smith, S. T. Elliot, T. J. Jones, T. A. Tombrello, and Q. Yu, Proc. SPIE **3019**, 241 (1997).
[22] S. Nikzad, Q. Yu, A. L. Smith, T. J. Jones, T. A. Tombrello, and S. T. Elliot, Appl. Phys. Lett. **73**, 3417 (1998).
[23] T. J. Jones, P. W. Deelman, S. T. Elliott, P. J. Grunthaner,R. Wilson, and S. Nikzad, Proc. SPIE **3965**, 148 (2000).
[24] S. Nikzad, *Scientific Charge-Coupled Devices*, edited by J. R. Janesick (SPIE, 2000), Vol. PM83.
[25] M. E. Hoenk, T. J. Cunningham, T. J. Jones, C. Wrigley, K. W. Newton, and S. Nikzad (unpublished).
[26] J. Blacksberg, M. E. Hoenk, T. Elliott, S. Holland, and S. Nikzad, Appl. Phys. Lett. **87**, 254101 (2005); J. Blacksberg, M. E. Hoenk, and S. Nikzad, J. Cryst. Growth **285**, 473 (2005).
[27] J. Janesick, T. Elliott, G. Fraschetti, S. Collins, M. Blouke, and B. Corrie, Proc. SPIE **1071**, 153 (1989).
[28] J. M. Jenkins, W. J. Barouki, E. W. Dunham, and J. S. McDonald, in *Planets Beyond Our Solar System and Next Generation Space Missions*, ASP Conference Series, Vol. 119, edited by D. Sodarblum (1997), pp. 277–280.
[29] J. C. Armitage, M. S. Dixit, J. Dubeau, H. Mes, and F. G. Oakham, in *The Measurement, Instrumentation, and Sensors Handbook*, edited by J. G. Websten (CRC, Boca Raton, FL, 1999), p. 67.
[30] J. F. Ziegler, J. P. Biersack, and U. Littmark, *The Stopping Power and Range of Ions in Matter* (Pergamon, New York, 1985).
[31] H. O. Funsten, S. M. Ritzau, R. W. Harper, and R. Korde, Appl. Phys. Lett. **84**, 3552 (2004).